engineering proceedings

MDPI

Proceedings

MMI Sensor for Diameter Measurement †

Victor Cardoso [1,2,*], Paulo Caldas [2,3], Maria Thereza Giraldi [4], Cindy Fernandes [5], Orlando Frazão [2,6], João Costa [1] and José Luís Santos [2,6]

1 Applied Electromagnetism Laboratory, Federal University of Pará, Rua Augusto Corrêa, 01, Belém 66075-110, Brazil
2 Institute for Systems and Computer Engineering, Technology and Science, Rua do Campo Alegre, 687, 4169-007 Porto, Portugal
3 Polytechnic Institute of Viana do Castelo, Rua Escola Industrial e Comercial de Nun'Álvares, 4900-347 Viana do Castelo, Portugal
4 Laboratory of Photonics, Military Institute of Engineering, Praça Gen. Tibúrcio, 80, Rio de Janeiro 22290-270, Brazil
5 Faculty of Computing and Electrical Engineering, Federal University of South and Southeast of Pará, Marabá 68507-590, Brazil
6 Department of Physics and Astronomy, Faculty of Sciences of University of Porto, Rua do Campo Alegre, 687, 4169-007 Porto, Portugal
* Correspondence: victorcard@ufpa.br
† Presented at the 8th Electronic Conference on Sensors and Applications, 1–15 November 2021; Available online: https://ecsa-8.sciforum.net/.

Abstract: Cylindrical structures analysis is important in several areas and can be performed through the evaluation of the diameter changes of these structures. Two important areas can be mentioned: pipelines for oil or gas distribution and, condition and growth of trees. In the tree diameter changes, the monitoring is directly related to irrigation, since it depends on the water soil deficit and trees are important in the global circulation of heat and water. This diameter can change in the order of 5 mm for some species. In this paper, it is proposed and experimentally investigated a strain gauge sensor based on a core diameter mismatch technique for diameter measurement. The sensor structure is formed by splicing an uncoated short section of MMF between two standard SMFs called SMF-MMF-SMF (SMS), the MMF length is 15 mm. Two cylindrical structures were developed on a 3D printer, with different diameter sizes (DS: 80 mm and 110 mm), to assist in monitoring the diameter changes. The SMS sensor was placed on the printed structure and fixed at two points such that by reducing the diameter of the structure, the sensor presents dips or peaks shift of the transmittance spectrum due to the induced curvature and strain. Three values were used for the spacing between the fixations points (FP): 5 mm, 10 mm and 15 mm. For DS = 80 mm, the sensor presents respectively: (a) a sensitivity of −0.876 nm/mm, R^2 of 0.9909 and a dynamic range of 5 mm; (b) a sensitivity of −0.3892 nm/mm, R^2 of 0.9954 and a dynamic range of 4 mm; and (c) a sensitivity of −0.768 nm/mm, R^2 of 0.9811 and a dynamic range of 2 mm. For DS = 110 mm, the sensor presents respectively: (a) a sensitivity of −0.22 nm/mm, R^2 of 0.9979 and a dynamic range of 8 mm; (b) a sensitivity of −0.2284 nm/mm, R^2 of 0.9888 and a dynamic range of 6 mm; and (c) a sensitivity of −0.691 nm/mm, R^2 of 0.9892 and a dynamic range of 3.5 mm.

Keywords: SMS; optical strain gauge; optical sensor; diameter monitoring

Citation: Cardoso, V.; Caldas, P.; Giraldi, M.T.; Fernandes, C.; Frazão, O.; Costa, J.; Santos, J.L. MMI Sensor for Diameter Measurement. *Eng. Proc.* **2021**, *1*, 0. https://doi.org/

Academic Editor: Firstname Lastname

Received:
Accepted:
Published: 1 November 2021

1. Introduction

Radial growth control is observed in several applications. In many areas, this monitoring plays an important role. For example, in the oil or gas transportation infrastructure the pressure in the pipeline is high, causing deformation and/or fatigue and consequently a disruption [1]. Pipelines deform when the deformation exceeds the established limit, which may be caused by the environment when natural disasters such as landslides and earthquakes occur or theft of material transported in pipelines happens. The corrosion

process is also one of the main factors contributing to accidents involving pipelines. In both cases, they can produce significant environmental damage, product loss, financial problems and sometimes the loss of life from explosions [2,3]. Another example, the monitoring of the tree diameter change is directly related to irrigation, since it depends on the soil water deficit and trees are important in the global circulation of heat and water, in addition, tree growth is affected by the CO_2 rate and air pollutants [4–8]. The use of optical sensors for these cases is interesting because they present characteristics such as immunity to electromagnetic interference, compact size, resistance to pressure, heat and corrosion, and the possibility of transmission over long distances.

Multimodal Interference (MMI) devices based on fiber optics have been extensively investigated in recent years for different applications as sensors to detect physical parameters such as temperature [9], strain [10], vibration [11], flow rate [12] and son on. Optical fiber sensors (OFS) offer many advantages: They are not susceptible to electromagnetic interference, low attenuation, lightweight, they can survive harsh environments and tolerate high temperatures. There are several types of MMI structures, such as Sagnac Interferometer [13] , Fabry-Perot Interferometer [14] and Singlemode-Multimode-Singlemode (SMS) structures [15]. The MMI structure most common is the SMS [15,16]. This structure is composed by a short segment of Multimode fiber (MMF) between two single-mode fibers (SMFs). The SMS sensor is based on the core diameter mismatch (CDM) technique and it consists of mode coupling mechanism to transfer optical power between the core mode and higher order modes of the cladding through mismatched sections. SMS Structures are most commonly used as sensors to detect physical parameters such as . SMS Structure in addition to presenting the advantages of optical fiber over conventional measurement technique, it also presents low cost of production, flexible design, ease of fabrication, compact size and high sensitivity [17–19].

In this work, we investigate a method for diameter monitoring using a traditional SMS structure. We use an experimental setup that uses the principle of the strain gauge based on SMS for diameter monitoring. We develop a structure in a 3D printer so that it was possible to perform the analysis of the diameter variation of different structures. The SMS sensor is put on the strain gauge and fixed on it in three points where the distance of fixed points is 5, 10 and 15 mm.

2. Experimental Setup

A traditional SMS structure, consists of a short MMF section spliced between two SMFs, as depicted in Figure 1. The light is injected from the input SMF into the MMF, where higher order and fundamental modes are excited, and interference between the different modes occurs while the light beam propagates along the MMF section [11,12]. Due to higher modes excitation, the optical power coupled to the output SMF depends on the amplitudes and phases of the MMF modes and this dictates the transmission spectral response at the output SMF. The MMF couples part of the light that travels along the core of the input SMF to the cladding of the output SMF, and this coupling induces a loss of power in the transmitted signal that travels along the core [20–22].

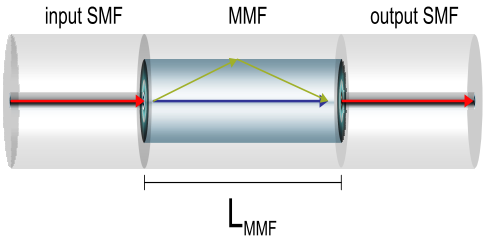

Figure 1. Schematic of the MMI sensor based on Core Diameter Mismatch technique.

In this work an experimental setup was proposed as shown in Figure 2. The transmission spectrum of the SMS sensor was monitored with an Optical Spectrum Analyzer (Anritsu, MS9740A). The sensors assembled in this work are fabricated with the core/cladding

diameters of the SMF 8.2/125 µm (Corning SMF-28, Inc.) and for the step-index MMF section, the core/cladding diameters are 105/125 µm (FG105-LCA from Thorlabs, Inc.). It is important to emphasize that for the lengths of the MMF section used in this work, it is now possible to observe the self imaging phenomenon because the length of the MMF is much shorter than the length needed to observe this phenomenon.

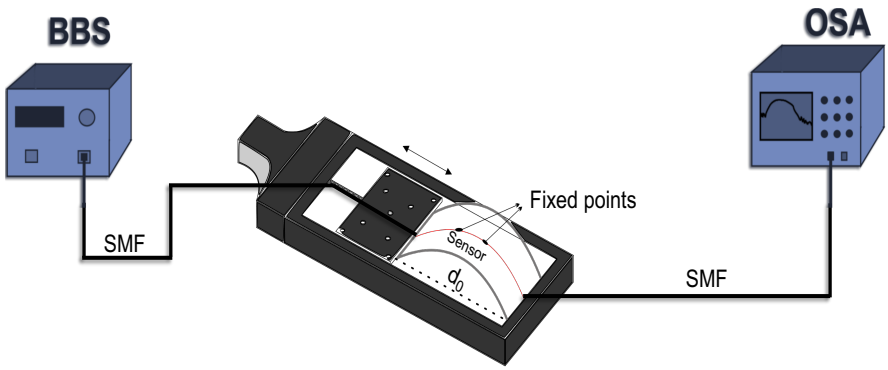

Figure 2. Schematic of the experimental setup for the diameter analysis that demonstrates the diameter reduction using a linear translation stage.

The MMFs lengths were 15 mm. Two cylindrical structures were developed on a 3D printer, with different diameter sizes (d_0), 80 mm and 110 mm, to assist in monitoring the diameter changes (Δd). The sensing head was fixed at two points on the pieces, with different distances between the fixed points. Three values were used for the spacing between the fixed points (FP), 5 mm, 10 mm and 15 mm. It was used a linear translation stage, to apply tension by moving the linear stage away from the fixed support. Thus, it is possible to introduce a strain in the sensor. The sensors present dips or peaks shift of transmittance spectrum due to the induced curvature and strain, as depicted in Figure 3.

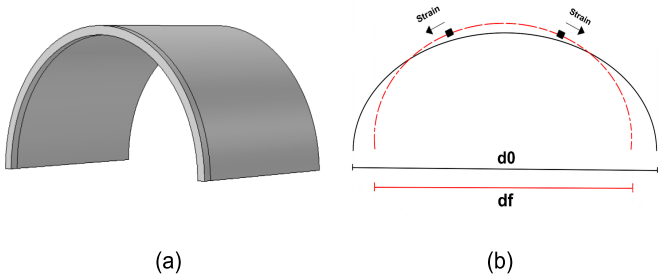

Figure 3. (**a**) Cylindrical structure developed on a 3D printer. (**b**) Mechanism of operation of the structure that demonstrates the diameter reduction.

3. Results and Discussion

The strain gauge with the SMS sensor was inserted in the linear stage transition that is controlled by computer. It was created a structure for monitoring the diameter using a 3D printer, as depicted in Figure 3a. This structure was created to simulate a radial change in structures such as pipelines and tree trunk which need to have their diameter monitored. A strain and curvature are applied on the optical fiber by reducing the diameter of the structure (d_0) and therefore it was possible to obtain the sensor response. This principle can be observed in Figure 3b. The diameters of the structures are 80 and 110 mm (d_0).

3.1. Structure Diameter with 80 mm

Firstly, the SMS sensor was placed on the cylindrical structure and it was fixed at 5 mm of the total length of the MMF section. Figure 4 shows the second-order polynomial fitting result of the corresponding wavelength shift as a function of displacement. It was

possible to obtain a sensitivity of -0.876 nm/mm, coefficient of determination (R^2) of 0.9909 and the dynamic range (Δd) of 5 mm, as depicted in Figure 4a. Figure 5a show the dip shift of the transmittance spectrum due to the induced curvature strain in $FP = 5$ mm. After that, the FP was increased to 10 mm. The R^2 showed a small increase, to 0.9954 as shown in Figure 4b. Figure 5b show the dip shift of the transmittance spectrum due to the induced curvature strain in $FP = 10$ mm. The sensitivity obtained for this configuration was -0.3892 nm/mm and the dynamic range of 4 mm. When the $FP = L_{MMF} = 15$ mm, it was possible to observe an increase in the sensitivity, of -0.768 nm/mm, when comparing with the result for $FP = 10$ mm. R^2 and dynamic range showed a reduction, respectively, to 0.9811 and 2 mm, as depicted Figure 4c. Figure 5c show the dip shift of the transmittance spectrum due to the induced curvature strain in $FP = 15$ mm.

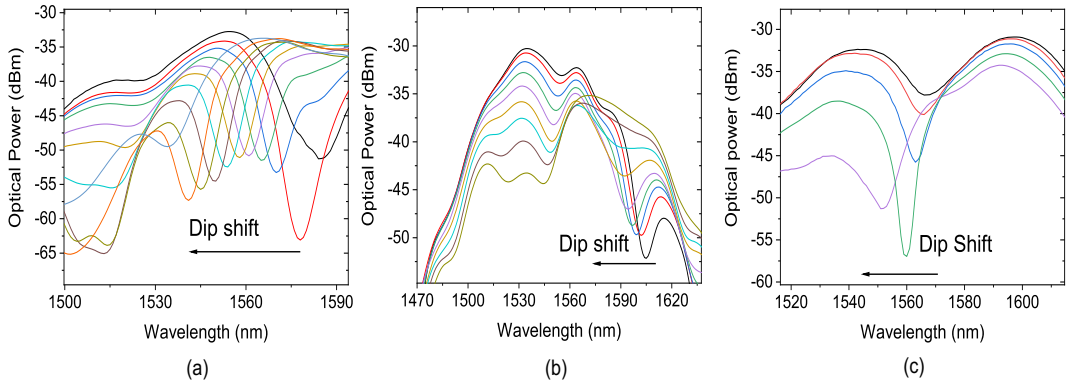

Figure 4. Wavelength shift as a function of displacement. (**a**) The sensor as $FP = 5$ mm and $DS = 80$ mm. (**b**) The sensor as $FP = 10$ mm and $DS = 80$ mm. (**c**) The sensor as $FP = 15$ mm and $DS = 80$ mm.

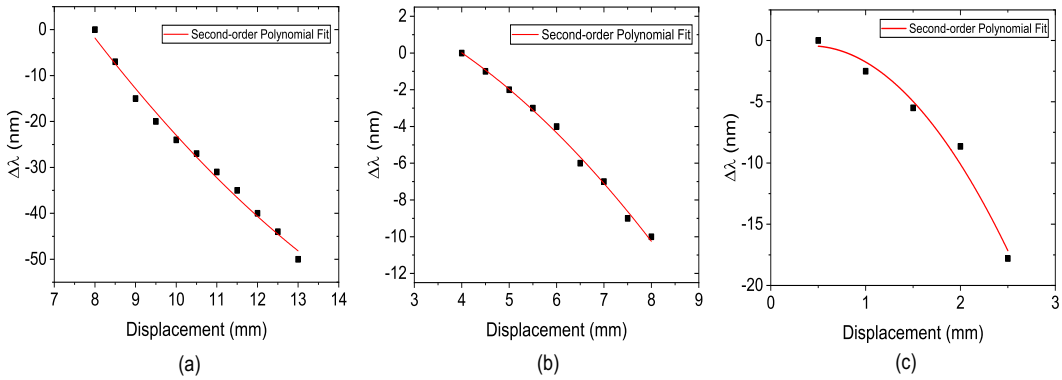

Figure 5. Transmission spectrum of the sensor. (**a**) The sensor as $FP = 5$ mm and $DS = 80$ mm. (**b**) The sensor as $FP = 10$ mm and $DS = 80$ mm. (**c**) The sensor as $FP = 15$ mm and $DS = 80$ mm.

3.2. Structure Diameter with 110 mm

The second part of the experiment is similar to what was performed previously. Figure 6 shows the second-order polynomial fitting result of the corresponding wavelength shift as a function of displacement. For the $FP = 5$ mm, it was possible to obtain a sensitivity of -0.22 nm/mm, R^2 of 0.9979 and dynamic range of 8 mm, as depicted in Figure 6a. Figure 7a show the peak shift of the transmittance spectrum due to the induced curvature strain in $FP = 5$ mm. After that, the FP was increased to 10 mm. The R^2 showed a decrease to 0.9888, as shown in Figure 6b. Figure 7b show the peak shift of the transmittance spectrum due to the induced curvature strain in $FP = 10$ mm. The sensitivity obtained for this configuration was -0.2284 nm/mm and the dynamic range of 4.5 mm. When $FP = L_{MMF} = 15$ mm, it was possible to observe an increase in the sensitivity of -0.691 nm/mm when comparing with the result for $FP = 10$ mm. The R^2 and dynamic

range showed a reduction, respectively, to 0.9892 and 3.5 nm, as depicted in Figure 6c. Figure 7c show the peak shift of transmittance spectrum due to induced curvature and strain in FP = 15 mm

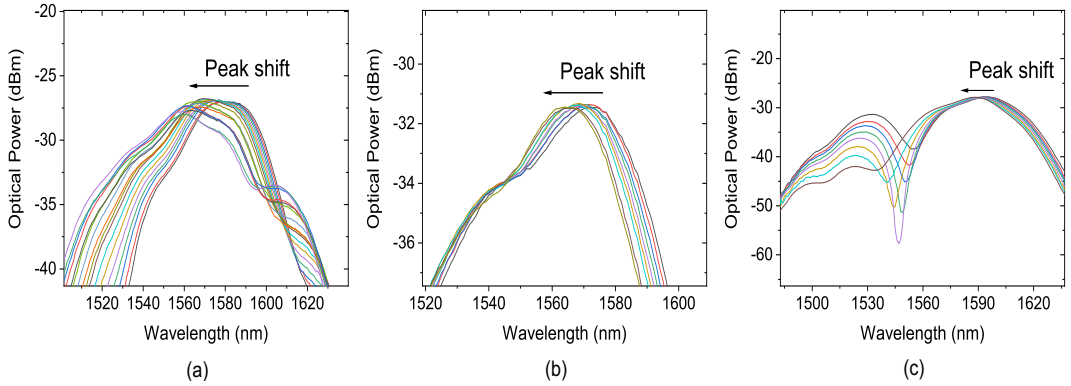

Figure 6. Wavelength shift as a function of displacement. (**a**) The sensor as $FP = 5$ mm and $DS = 110$ mm. (**b**) The sensor as $FP = 10$ mm and $DS = 110$ mm. (**c**) The sensor as $FP = 15$ mm and $DS = 110$ mm.

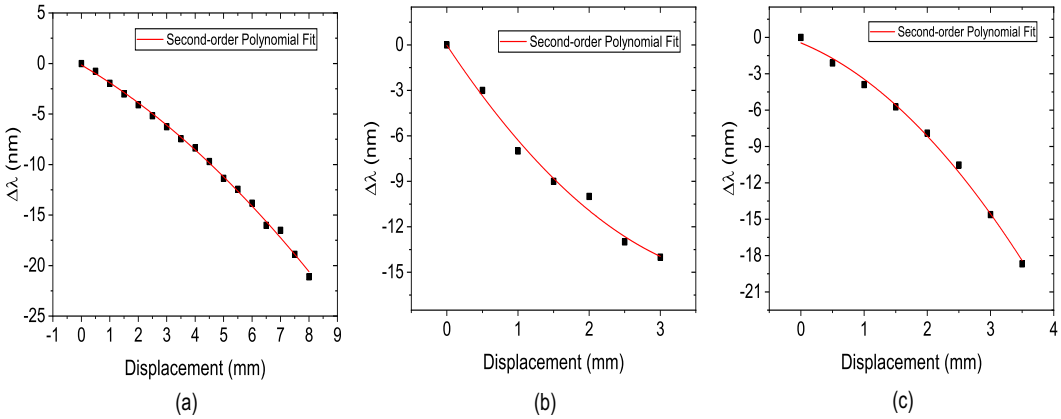

Figure 7. Transmission spectrum of the sensor. (**a**) The sensor as $FP = 5$ mm and $DS = 110$ mm. (**b**) The sensor as $FP = 10$ mm and $DS = 110$ mm. (**c**) The sensor as $FP = 15$ mm and $DS = 110$ mm.

4. Conclusions

In conclusion, we proposed an experimental investigation about the strain gauge based on traditional MMI structure, it is the SMS sensor, for diameter monitoring. We developed an experimental setup for this investigation. The fabrication of the setups and the proposed sensor are simple and repeatable. The results demonstrate that it is possible to monitor the diameter using the strain gauge based on SMS sensor proposed in this work. The results present good sensitivities values, excellent coefficient of determination and dynamics ranges with several possibilities to practical application such as in pipelines and tree trunk growth. This study presents preliminary results and the next step will be to analyze other possible configurations since with the correct arrangement, it is possible to optimize the structure and their characteristics.

Institutional Review Board Statement:

Informed Consent Statement:

Data Availability Statement:

Acknowledgments: This study was financed in part by the Brazilian Funding Agencies Conselho Nacional de Desenvolvimento Científico e Tecnológico (CNPq) and Coordenação de Aperfeiçoamento de Pessoal de Nível Superior (CAPES). It was supported by the Federal University of Pará (UFPA) and the Military Institute of Engineering (IME) from Brazil and the Institute for Systems and Computer

Engineering, Technology and Science (INESC TEC) and the Department of Physics and Astronomy, Faculty of Sciences of University of Porto from Portugal.

Conflicts of Interest: The authors declare no conflict of interest.

References

1. Amaro, R.L.; Drexler, E.S.; Slifka, A.J. Fatigue crack growth modeling of pipeline steels in high pressure gaseous hydrogen. *Int. J. Fatigue* **2014**, *62*, 249–257, doi:10.1016/j.ijfatigue.2013.10.013.
2. Yanga, Y.; Hongb, C.; Abrob, Z.A.; Wanga, L.; Yifan, Z. A new Fiber Bragg Grating sensor based circumferential strain sensorfabricated using 3D printing method. *Sensors Actuators A Phys.* **2019**, *295*, 663–670.
3. Ren, L.; guang Jia, Z.; nan Li, H.; Song, G. Design and experimental study on FBG hoop-strain sensor in pipeline monitoring. *Opt. Fiber Technol.* **2014**, *20*, 15–23.
4. Cohen, M.; Goldhamer, D.A.; Fereres, E.; Girona, J.; Mata, M. Assessment of peach tree responses to irrigation water ficits by continuous monitoring of trunk diameter changes. *J. Hortic. Sci. Biotechnol.* **2001**, *76*, 55–60.
5. Martín-Palomo, M.; Corell, M.; Girón, I.; Andreu, L.; Trigo, E.; López-Moreno, Y.; Torrecillas, A.; Centeno, A.; Pérez-López, D.; Moriana, A. Pattern of trunk diameter fluctuations of almond trees in deficit irrigation scheduling during the first seasons. *Agric. Water Manag.* **2019**, *218*, 115–123, doi:10.1016/j.agwat.2019.03.033.
6. Çakir, R. Effect of water stress at different development stages on vegetative and reproductive growth of corn. *Field Crop. Res.* **2004**, *89*, 1–16, doi:10.1016/j.fcr.2004.01.005.
7. Corella, M.; Martín-Palomoa, M.; Girónb, I.; Andreua, L.; Galindoa, A.; Centenod, A.; Pérez-Lópezd, D.; Morianaa, A. Stem water potential-based regulated deficit irrigation scheduling for olive table trees. *Agric. Water Manag.* **2020**, *242*, 106418.
8. Goldhamer, D.A.; Fereres, E. Irrigation scheduling of almond trees with trunk diameter sensors. *Irrig. Sci.* **2004**, *23*, 11–19.
9. Wang, Q.; Meng, H.; Fan, X.; Zhou, M.; Liu, F.; Liu, C.; Wei, Z.; Wang, F.; Tan, C. Optical fiber temperature sensor based on a Mach-Zehnder interferometer with single-mode-thin-core-single-mode fiber structure. *Rev. Sci. Instrum.* **2020**, *91*, 015006.
10. Fernandes, C.S.; Rocco Giraldi, M.T.M.; de Sousa, M.J.; Costa, J.C.W.A.; Rodrigues, L.D.; da Silva, F.R.B.; Ferreira, G.F.; dos Reis, R.A.N. Strain sensing based on a core diameter mismatch structure. *Microw. Opt. Technol. Lett.* **2019**, *61*, 2013–2019.
11. Fernandes, C.S.; Giraldi, M.T.M.R.; de Sousa, M.J.; Costa, J.C.W.A.; Gouveia, C.; Jorge, P.; Franco, M.A.R. Curvature and Vibration Sensing Based on Core Diameter Mismatch Structures. *IEEE Trans. Instrum. Meas.* **2016**, *65*, 2120–2128.
12. Costa, J.; Franco, M.A.; Serrão, V.A.; Cordeiro, C.M.; Giraldi, M.T. Macrobending SMS fiber-optic anemometer and flow sensor. *Opt. Fiber Technol.* **2019**, *52*, 101981.
13. Ruan, J. Fiber curvature sensor based on concave-heterotypic cascaded fiber Sagnac interferometer. *Microw Opt Technol Lett.* **2020**, *62*, 3645–3649.
14. Li, X.; Chen, N.; Zhou, X.; Gong, P.; Wang, S.; Zhang, Y.; Zhao, Y. A review of specialty fiber biosensors based on interferometer configuration. *J. Biophotonics* **2021**, *14*, e202100068.
15. Wu, Q.; Qu, Y.; Liu, J.; Yuan, J.; Wan, S.P.; Wu, T.; He, X.D.; Liu, B.; Liu, D.; Ma, Y.; Semenova, Y.; Wang, P.; Xin, X.; Farrell, G. Singlemode-Multimode-Singlemode Fiber Structures for Sensing Applications—A Review. *IEEE Sensors J.* **2021**, *21*, 12734–12751, doi:10.1109/JSEN.2020.3039912.
16. Wang, K.; Dong, X.; Köhler, M.H.; Kienle, P.; Bian, Q.; Jakobi, M.; Koch, A.W. Advances in Optical Fiber Sensors Based on Multimode Interference (MMI): A Review. *IEEE Sensors J.* **2021**, *21*, 132–142, doi:10.1109/JSEN.2020.3015086.
17. Korposh, S.; James, S.W.; Lee, S.W.; Tatam, R.P. Tapered Optical Fibre Sensors: Current Trends and Future Perspectives. *Sensors* **2019**, *19*, 2294.
18. Lu, X.; Thomas, P.J.; Hellevang, J.O. A Review of Methods for Fibre-Optic Distributed Chemical Sensing. *Sensors* **2019**, *19*, 2876.
19. Roriz, P.; Silva, S.; Frazão, O.; Novais, S. Optical Fiber Temperature Sensors and Their Biomedical Applications. *Sensors* **2020**, *20*, 2113.
20. Wu, Q.; Semenova, Y.; Wang, P.; Farrell, G. High sensitivity SMS fiber structure based refractometer - analysis and experiment. *Opt. Express* **2011**, *19*, 7937–7944.
21. Wang, Q.; Farrell, G.; Yan, W. Investigation on single-mode-multimode-single-mode fiber structure. *J. Light. Technol.* **2008**, *26*, 512–519.
22. Li, Y.; Liu, Z.; Jian, S. Multimode interference refractive index sensor based on coreless fiber. *Photonic Sensors* **2014**, *4*, 21–27.